Nanoscale

Accepted Manuscript

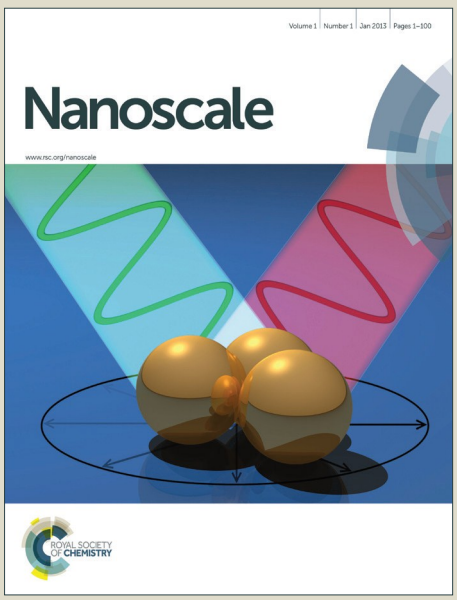

ROYAL SOCIETY OF CHEMISTRY

www.rsc.org/nanoscale

Journal Name RSCPublishing

ARTICLE

Laser Beam Controlled Drug Release from Ce6-Gold Nanorods Composites in Living Cells: A FLIM Study

Cite this: DOI: 10.1039/x0xx00000x

Yongkui Xu*, Ruoyu He, Dongdong Lin, Minbiao Ji*, Jiyao Chen

Received 00th January 2012,
Accepted 00th January 2012

DOI: 10.1039/x0xx00000x

www.rsc.org/

A new method to image drug release from drug-nanoparticle composite in living cells was established. The composites of silica coated gold nanorods (AuNR@SiO_2) and chlorine e6 (Ce6) photosensitizer (AuNR@SiO_2-Ce6) were formed by electrostatic force with the Ce6 loading efficiency of 80%. The strong resonance absorptions of AuNR@SiO2-Ce6 in the near-infrared (NIR) region enabled effective release Ce6 from AuNR@SiO_2-Ce6 by 780 nm CW laser irradiation. The 780 nm laser beam was applied to not only control the releasing amount of Ce6 from cellular AuNR@SiO_2-Ce6 by adjusting the irradiation dose (time), but also spatially confine the Ce6 release in cells by focusing the laser beam on the target sites. Furthermore, the fluorescence lifetime of Ce6 was found to change drastically from 0.9 ns in the AuNR@SiO_2-Ce6 complex to 6 ns after release, and therefore fluorescence lifetime imaging microscopy (FLIM) was introduced to image the photo-induced Ce6 release in living cells. Finally, controllable killing effect of photodynamic cancer therapy (PDT) using AuNR@SiO_2-Ce6 was demonstrated by changing the released amount of Ce6, which indicates that AuNR@SiO_2-Ce6 is promising for targeted tumour PDT.

1. Introduction

With the rapid development of nanotechnology, nanoparticles have been suggested as the carriers for efficient drug delivery because of their versatile physical and chemical properties[1-4]. Some nanovehicles such as mesoporous silica nanoparticles are able to load a great amount of drugs and release them in living systems by slow diffusion[1, 5, 6]. However, for these nanoparticles, the controlled release in targeted sites of living body is difficult to reach and better strategies are needed[7]. Gold nanoparticles have been widely used in biomedicine researches[8] such as metal enhanced fluorescence [9-12] and photothermal therapy [13, 14], due to its chemical inertness, minimum biological toxicity and strong light absorption resulted from the Surface Plasmon Resonance (SPR) [15]. Gold nanocubes can bring two orders of magnitude fluorescence enhancement of aluminium phthalocyanine.[15] Gold nanorods (AuNRs) can be used in photo-thermal therapy of cancers and even used as nanobombs to destroy cancer cells under the irradiation of NIR femtosecond (fs) laser[16]. With suitable aspect ratios of about 4-5, the AuNRs have strong absorption in the NIR region, which is the so-called tissue optical window, because of superior light penetration. Importantly, the photothermal effect of AuNRs allows controllable drug release from the AuNR-drug composites through spatial and temporal management of NIR light irradiation[17-19]. The ideal of using AuNRs to release the drugs by light sounds reasonable. However, quantitative measurement of released drugs from AuNR-drug is a great challenge. If the releasing measurement is not established, the potential of this modality for controlled drug release cannot be evaluated. In this work, we have established a method of imaging drug release in living cells by fluorescence lifetime imaging microscope (FLIM) based on the fact that certain drug fluorescence lifetime remarkably vary along different position with respect to the AuNRs.[20] Herein a well-known photosensitizer for photodynamic therapy (PDT) of cancers, chlorin e6 (Ce6), was applied as the fluorescent drug. Our results confirmed that FLIM is a powerful tool to study the releasing process of Ce6 from AuNR@SiO_2-Ce6 composites in living cells by controlling the irradiation does of 780 nm laser. Furthermore, the in vitro PDT experiments showed that the PDT effect of the AuNR@SiO_2-Ce6 composites can be administrated by controlling the released amount of Ce6. The controllable PDT effect would be very useful in PDT practice by photo-releasing photosensitizers from composite carriers in tumour site only and thus preventing the skin photo-toxicity.

2. Results and discussion

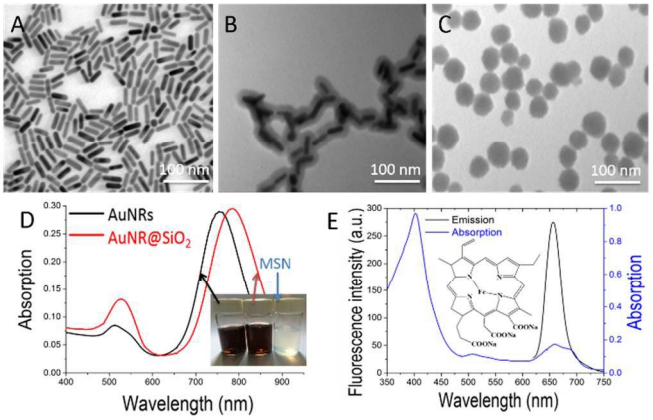

Fig. 1. Characterization of AuNRs, AuNR@SiO_2 and MSNs. A, B and C are their corresponding TEM images. D shows the absorption spectra of AuNRs and AuNR@SiO_2 and pictures of AuNRs, AuNR@SiO_2 and MSNs in aqueous solutions. E shows the molecular structure of Ce6 and the absorption and fluorescence spectra of Ce6 with concentration of 5 μM under excitation of 405 nm.

The CTAB-stabilized gold nanorods, amino group modified mesoporous silica shell coated gold nanorods (AuNR@SiO_2) and amino group modified mesoporous silica nanoparticles (MSNs) were prepared. The characterization of as-prepared nanoparticles was taken. The TEM images of AuNRs, AuNR@SiO_2 and MSNs are shown in Figure 1(A, B and C). The size of particles synthesized were about 50 nm. The optimal goal of targeted drug delivery is to deliver active drugs to specific tumour sites while minimizing the side effects of the drugs on normal tissues. One way to do this is via active tumour targeting through receptor-mediated endocytosis by modifying the surface of nanoparticles with ligands. [21] However, such an approach has been questioned for drawbacks that limit its efficacy, such as decreases blood circulation time and reduced tumour penetration.[22] In this work, we chose to use the passive targeting approach. Due to the enhanced permeability and retention (EPR) effect of tumour tissues, nanoparticles could selectively penetrate through the defective tumour vasculatures accumulating in tumours, achieving targeted deliveries.[23] So instead of modifying the surface of nanoparticles with ligands, we modified the surface with amino group, making it positively charged for cell endocytosis easier The AuNRs have two SPR bands with the transverse surface plasmon resonance(TSPR) band at 530 nm and the longitudinal surface plasmon resonance(LSPR) band around 760 nm, corresponding to the aspect ratio of 3.7, according to the absorption spectrum showed in figure 1(D). Compared with the absorption spectrum of AuNRs, AuNR@SiO_2 shows an enhanced absorption at TSPR and a red shift band of LSPR at 780 nm. The MSNs absorb little visible lights and appear milky.

In this work, we used a soluble form of Ce6 derivative - sodium iron chlorophyllin, which was still named Ce6 for convenience. The molecular structure was shown in figure 1E.The absorption and fluorescence spectra are also exhibited in Figure 1E. The Ce6 has two absorption bands located around 405 nm (B band) and 660 nm (Q band), and its fluorescence band is at 660 nm. Since each Ce6 molecule possesses 3 negative charged side carboxylic groups, it is easy to bind on the surface of positively charged nanoparticles to form conjugates. Although the CTAB stabilized AuNRs can well disperse in aqueous solution and conjugate with Ce6, the toxicity of CTAB is a great concern. Therefore, we coated the AuNRs with the biocompatible silica shells making the AuNR@SiO_2 for less toxicity with increased drug loading ability.

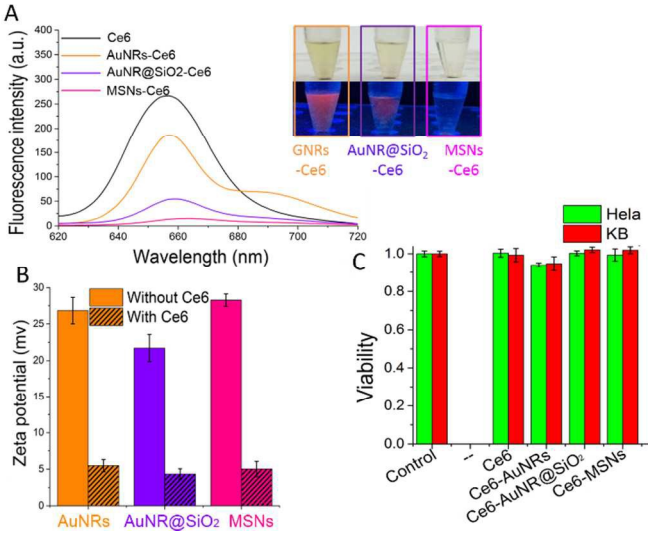

Fig. 2. (A) The comparison of Ce6 loading of three kinds of nanoparticles by measuring the fluorescence of un-conjugated Ce6 left in the supernatant fluid of each composites after centrifugation. The upper row of insert shows the common photos of these samples and the low row of the insert gives the fluorescence photographs of the supernatants of these samples under the irradiation of an UV beam of 365 nm. (B) Zeta potentials of AuNRs, AuNR@SiO_2, MSNs before and after Ce6 conjugation. (C) Cytotoxicities of used compounds on Hela and KB cells. The incubation concentration of Ce6 was 5 μM and those of composites of Ce6 to nanoparticles were 5 μM to 30 pM and the incubation time was 2 hours. The control groups were cells without any treatment.

The Ce6 loading experiment was carried out consequently. The loading ability of each kind of nanoparticles can be measured by the fluorescence comparison of Ce6 before and after loading. After mixing 5 μL 1 mM Ce6 with 0.3 mL 100 pM AuNRs, AuNR@SiO_2 or MSNs, respectively, and shaking for overnight, the composites of AuNRs-Ce6, AuNR@SiO_2-Ce6 and MSNs-Ce6 were formed. These composite samples were centrifuged to separate the composites at the bottom of the centrifuging tube and the unloaded free Ce6 in the supernatant. By comparing the fluorescence intensity of these unloaded Ce6 in the supernatant for each case with that of Ce6 at the original concentration (5 μM) before the conjugation, the Ce6 loading ratio for each case can be evaluated. As shown in Figure 2A, the loading ratios were obviously different for these composites which can be seen from the fluorescence spectra/intensities comparison and the visual observation under UV excitation. According to the following formula (1)

$$loading\ ratio = 1 - \frac{\text{fluorescence intensity of supernatant}}{\text{fluorescence intensity of 5 μM Ce6}} \quad (1)$$

The loading ratio can be calculated. For the MSNs-Ce6 composites, the loading ratio reached 95% demonstrating that the MSNs were good drug carriers. The loading ratio of AuNR@SiO_2-Ce6 was 80%, much higher than that of AuNRs-Ce6 (34%), indicating that AuNR@SiO_2-Ce6 was also a suitable composite for Ce6 loading.

Since these three kinds of nanoparticles were all positively charged, their Zeta potentials were in the region of +20 - +30 mV. When Ce6 molecules (5μM) were linked to these nanoparticles, Zeta potentials of the composites all decreased to about +5 mV (Figure 2B), indicating that the conjugation was established. The cytotoxicities of these composites were measured using Hela and KB cell lines as in vitro models. As shown in Figure 2C, after 2 hours incubation the observable toxicity can be seen for the

AuNR-Ce6 composites which induced 10% cell damaging. Such toxicity of AuNR-Ce6 is reasonable as the surface CTAB of AuNRs was known as the toxic agent. The toxicity of AuNR@SiO_2-Ce6 was reduced as almost no significant damaging could be found. The silicon shell is much safer than CTAB, so that the AuNR@SiO_2-Ce6 was selected for next-step drug releasing experiments.

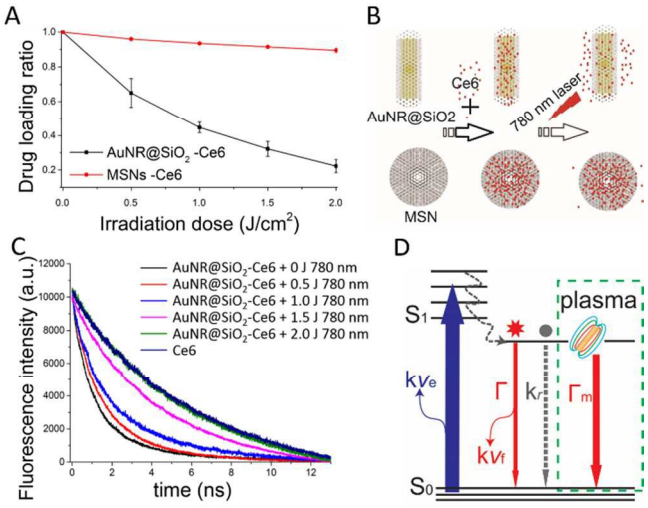

Fig. 3. (A) Comparison of Ce6 releases from AuNR@SiO_2-Ce6 and MSN-Ce6 in aqueous solutions under the irradiation of 780 nm laser. (B) The sketch map of Ce6 loading and release by AuNR@SiO_2 and MSNs. (C) Fluorescence lifetime changes of AuNR@SiO_2-Ce6 aqueous solution under the irradiation of 780 nm laser with different doses. D）Energy level diagram and schematic representation of energy transfer path involved in AuNR-enhanced of Ce6.

Since the LSPR band of AuNRs locates at 780 nm, the irradiation of 780 nm laser may produce photo-thermal effect on AuNRs to increase the temperature of AuNRs, resulting in the Ce6 release from the AuNR@SiO_2-Ce6. A middle power of 100 mW 780 nm laser was used to irradiate the composite aqueous solutions. After a certain dose irradiation, the composite solution was centrifuged to separate the supernatant and the AuNR@SiO_2-Ce6 composite at the bottom of the centrifuging tube, and then the supernatant was collected for fluorescence intensity measurement to determine the released amount of Ce6 in the supernatant. The releases of two composites of AuNR@SiO_2-Ce6 and MSNs-Ce6 in aqueous solution were studied. As shown in Figure 3A, no obvious release of Ce6 could be found for MSN-Ce6 after 780 nm laser irradiations, because the MSNs have little absorption at 780 nm and thus the photothermal effect can be neglected. Therefore, the MSNs are not good candidates for light controlled drug release study. With the increased irradiation dose of the 780 nm laser, the Ce6 release from AuNR@SiO_2-Ce6 was enhanced accordingly and a remarkable release (80%) of Ce6 molecules reached after 2 J dose irradiation of 780 nm laser, indicating that AuNR@SiO_2 composites are suitable carriers for light controlled drug release. Such releasing courses are sketched in Figure 3B. This result confidently demonstrates that the 780 nm laser can conveniently control the Ce6 release from AuNR@SiO_2-Ce6 in aqueous solution. However, the interesting point for drug release is that how to measure such controlled release in living systems. The above fluorescence intensity measurement in supernatant after the irradiation is certainly not suitable for living systems and other detection ways to measure the controlled release are needed to be established. Based on the theory of metal-enhanced fluorescence (MEF), the SPR in metal particles brings a new radiative rate Γ_m to attached fluorophores, and thus the lifetime τ of the fluorophores is shortened as described with the radiative rate Γ and non- radiative rate k_{nr} in the following formula.[24]

$$\tau=1/(\Gamma_m+\Gamma+k_{nr}) \quad (2)$$

The fluorescence lifetimes of free Ce6 and conjugated Ce6 in AuNR@SiO_2-Ce6 in aqueous solution were measured firstly to confirm the lifetime difference of two cases. As shown in Figure 3C, the fluorescence lifetime of un-conjugated Ce6 is 6.29 ns, whereas that of conjugated Ce6 is greatly shortened to 0.91 ns. Therefore the fluorescence lifetime difference can be used to measure the Ce6 release from AuNR@SiO_2-Ce6 composites. As shown in Figure 3A, under the irradiation of 780 nm laser the conjugated Ce6 gradually released from the AuNR@SiO_2-Ce6. In these situations, the solutions contained released free Ce6 and conjugated Ce6 in AuNR@SiO_2-Ce6 so that the fluorescence lifetime of the solution should be the average of two components according to their corresponding percentages. With the increased irradiation dose of 780 nm laser, the fluorescence lifetime gradually approached that of free Ce6. With the irradiation dose of 2 J, the fluorescence lifetime curve was almost overlapped with that of free Ce6 totally (Figure 3C), because in this situation most Ce6 molecules had been released into solution. Based on these results, the fluorescence lifetime change can be used as a sensitive tool to further measure the Ce6 releasing from AuNR@SiO_2-Ce6 in living cells in situ.

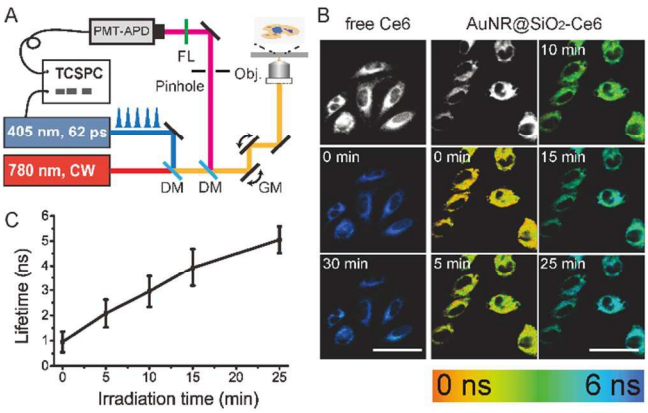

Fig. 4. (A) Setup schematics of the fluorescence lifetime and FLIM experiments. (B) Fluorescence images of KB cells incubated with free Ce6 (first column) and AuNR@SiO_2-Ce6 (second and third column). Fluorescence intensity images are shown in gray, and FLIM images of these cells under different irradiation times of 2 mW 780 nm laser are shown in false-colour with the colour map indicating the fluorescence lifetime. (C) The time-dependent mean fluorescence lifetime of all pixels in fluorescence lifetime images of AuNR@SiO_2-Ce6 incubated KB cells after irradiation. DM: dichroic mirror, GM: galvo mirror, FL: filter. Scale bar: 100 μm.

Our experiment setup is shown in Figure 4A. A 780 nm CW laser was introduced into the microscope as the controlling light for Ce6 release from cellular AuNR@SiO_2-Ce6, another 405 nm picosecond (ps) pulsed laser was used for fluorescence excitation. By measuring the time elapsed between excitation laser pulses and fluorescence photons with time-correlated single-photon counting (TCSPC), we can calculate the lifetime of the excited fluorophores at each laser focus. A fluorescence lifetime imaging microscope (FLIM) therefore maps the fluorescence lifetimes pixel by pixel as

the laser scans through the sample by a pair of galvo mirrors. FLIM is practicable for imaging fluorescence lifetime changes during relatively slow (normally >30 s) dynamic processes in a small area giving the quasi real time mapping of fluorescence lifetime in living cell.[25] After incubation with free Ce6 (5 μM) or AuNR@SiO_2-Ce6 (20 pM-5 μM) the drug loaded KB cells were measured with FLIM, while a 2 mW 780 nm laser was used to photo-release Ce6 from AuNR@SiO2-Ce6 (Fig. 4B). As a control, the fluorescence lifetimes of Ce6 in free Ce6 treated KB cells maintained around 6 ns before and after 30 min of the 780 nm irradiation. On the contrary, the fluorescence lifetimes of Ce6 in AuNR@SiO_2-Ce6 incubated KB cells changed gradually from 0.9 ns to 5 ns as the irradiation time of 780 nm laser increased to 25 min. Such changes could be clearly seen in the false-coloured FLIM images in Figure 4B, indicating that Ce6 molecules were released from cellular AuNR@SiO_2-Ce6 composites under 780 nm laser irradiation. Figure 4C shows the statistical change of Ce6 lifetimes of AuNR@SiO_2-Ce6 composites incubated cells under the irradiation for different times. These results demonstrated for the first time that FLIM could serve as a powerful tool to measure the dynamic fluorescent drug release from plasma particles in vitro.

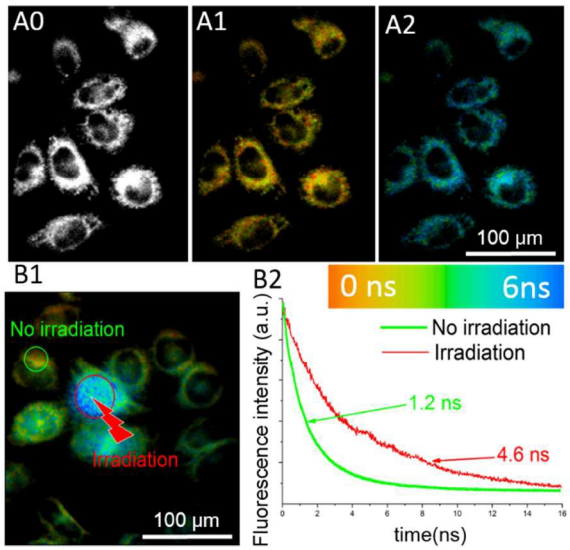

Fig. 5 (A) The fluorescence intensity image of AuNR@SiO_2-Ce6 incubated Hela cells (A0) and corresponding fluorescence lifetime images of cells before (A1) and after (A2) irradiation of 2 mW 780 nm laser for 30 minutes with a repetitive x-y scanning mode. (B) The fluorescence lifetime images of AuNR@SiO_2-Ce6 incubated cells after the irradiation of 2 mW 780 nm laser for 3 minutes with a point-scan mode. (B1). In B1, a red circle marked part of a cell had been irradiated by 780 nm laser before the FLIM image acquired. B2 shows the fluorescence lifetime decay curves of the 780 nm laser irradiated area and un-irradiated area (green circled areas) in B1.

Figure 5A shows the FLIM images of Ce6-AuNR@SiO_2 in another cell line (Hela cells) before and after irradiation of 780 nm laser for 30 min. Statistically, from figure 5A1 to 5A2, the average fluorescence lifetime was about 1 ns before the irradiation and turned to be 4.6 ns after the irradiation of 2 mW 780 nm laser for 30 minutes, confirming the Ce6 released from AuNR@SiO2-Ce6 conjugates. To further demonstrate the precise control of Ce6 release in cells by the 780 nm laser, we used point-scan model (without scanning) to irradiate a select small area on a cell with the 780 nm laser for 3 min leaving the other area un-irradiated, and then the FLIM image of these cells were acquired as shown in Figure 5B1. The blue colour (with the lifetime of about 5 ns) of 780 nm laser irradiated area obviously differs with the yellow-green colour (with the lifetime of around 1 ns) of un-irradiated regions. Figure 5B2 gives the fluorescence lifetimes of 780 nm irradiated area and un-irradiated region as circled in Figure 5B1, and the corresponding lifetimes of 4.6 ns and 1.2 ns support that the 780 nm laser beam can control the Ce6 release in the micro-region of the living cell. When a 2 mW light was tight-focused into a micrometres area (power density ~200kW/cm^2) and with continuous irradiation the damage becomes obvious, which can be seen from figure 5(B1) where the nucleus of the cell chosen to irradiate was destroyed. Due to the fact that absorption efficiency of AuNRs depends greatly on the distribution and arrangement, there is no accurate temperature rise calculation method with irradiation. Here we estimate the temperature of AuNRs in water solution under continuous 780 nm irradiation by following calculation using the steady state thermal diffusion equation.

$$P_{\mathrm{I}} \cdot \sigma_{\mathrm{AuNRs}} = G_{\mathrm{Au-water}} S_{\mathrm{AuNR}} (T_{\mathrm{AuNR}} - T_{water}) \quad (3)$$

Where T_{AuNR} and T_{water} are the temperatures of AuNRs and water surroundings, which is set as 300K considering the high heat capacity of water and highvolume ratio of water to AuNRs. The laser energy absorbed by AuNRs depends on the laser fluence P_{I}, and the absorption cross-sectional area σ_{AuNR}. $G_{\mathrm{Au\text{-}water}}$ is the thermal conductance at the AuNR/water interface. S_{AuNR} is the surface area of the AuNRs. And according to the system parameters and properties of nanoparticles, we can get an approximate temperature of 1100 K of AuNRs which is high enough to scald the cell apparatus. But with the x-y repeat scan model, there is only 4.3 μs 780 nm irradiation for every pixel in each circle. Considering the heat diffusion to the water solution in the laser focus together with the concentration of AuNRs, supposed to be 1 μM, the temperature of surroundings rise less than 1 K, giving little thermal damage on cells.

To cure the localized disease, specifically targeted drug delivery is the goal of medical researchers. However, so far the targeting effect of drugs is still limited due to the complexity of living systems. Generally, when drugs are delivered into living body, the drugs reach both diseased site and normal tissues inducing the therapy effect and causing the side-effect on normal tissue probably. The controlled drug delivery is a promising strategy of drug delivery by using a carrier to load drugs and releasing drugs from the carrier only in diseased site with a controlled manner. The controlled drug delivery can certainly decrease the side-effect and improve the therapeutic effect by efficient and thorough drug-release, but it is challenged by the controlled manner used which should be feasible and practicable. In this work, we found that the AuNR@SiO_2 are suitable carriers and the NIR laser beam irradiation is the good way to release the drugs from AuNR@SiO_2-Drug composites due to the strong absorptions at LSPR band. With the AuNR@SiO_2-Ce6, the effective light controlled Ce6 release was achieved in vitro here.

The purpose of controlled drug release is to release the drugs in desired site for therapy. The ability of AuNR@SiO_2-Ce6 to release Ce6 for therapy was checked then. The Ce6, a photosensitizer, is known as an efficient $^1O_2$ producer. The PDT effects of Ce6 and AuNR@SiO_2-Ce6 all depend on their $^1O_2$ production. In this work, the AuNR@SiO_2-Ce6 was designed as a poor $^1O_2$ producer due to the short-distance reactive agent because of its short lifetime of $^1O_2$, and the photo-released Ce6 from AuNR@SiO_2-Ce6 was the good $^1O_2$ generator. Using DBPF as the sensitive $^1O_2$ probes, the $^1O_2$

production of AuNR@SiO_2-Ce6 in aqueous solution was measured when the sample solution had been irradiated by the 650 nm light beam which is at the absorption Q band of Ce6. Figure 6A shows that the $^1O_2$ production of AuNR@SiO_2-Ce6 aqueous solution (without pre-irradiation of 780 nm laser) under the irradiation of 650 nm light beam is relatively low as expected. When Ce6 was captured in mesoporous silica shell of AuNR@SiO_2, the excited Ce6 has less chance to collide with O_2 to produce $^1O_2$ because only a small amount of O_2 diffused into the mesoporous silica shell. Moreover even $^1O_2$ was produced in mesoporous silica shell such $^1O_2$ would disappear before it encountered and oxidized the DBPF, because of the same reason as only a small amount of DBPF existed in mesoporous silica shell. When the Ce6 was photo-released from the AuNR@SiO_2-Ce6 by the pre-irradiation of 780 nm laser, the $^1O_2$ production should be increased. For the sample solution of AuNR@SiO_2-Ce6 which has been pre-irradiated by the 780 nm laser with the irradiation dose of 2 J to release most attached Ce6, the $^1O_2$ production is so obvious that the DBPF was rapidly degraded with the irradiation of 650 nm light (Figure 6B). For the sample solution of AuNR@SiO_2-Ce6 which has been pre-irradiated by the 780 nm laser with the irradiation dose less than 2 J, the DBPF degradation rate is relatively lower than that in Figure 6B and summarized in Figure 6C. Therefore, the photosensitization ability of AuNR@SiO_2-Ce6 can be modified by controlling the Ce6 release from AuNR@SiO_2-Ce6 with the pre-irradiation of a 780 nm laser beam. The controllable photosensitization ability of AuNR@SiO_2-Ce6 would be very useful in PDT applications as we can only release the Ce6 from AuNR@SiO_2-Ce6 in tumour site by the irradiation of a 780 nm laser beam and thus decrease the photo-toxicity in normal tissues.

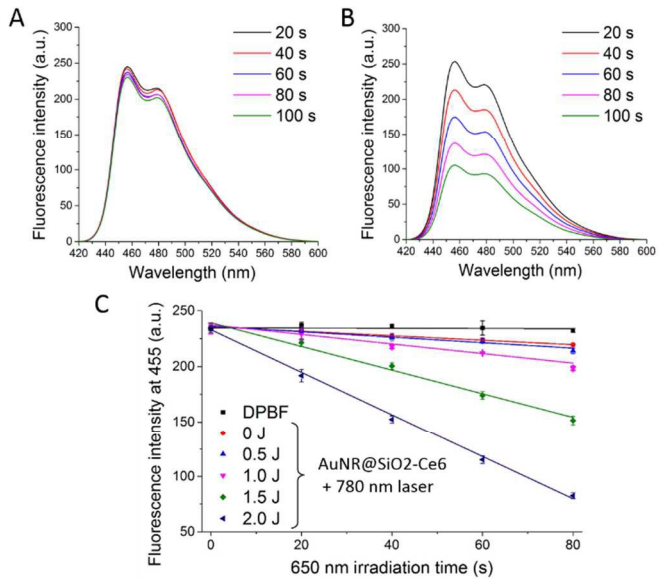

Fig. 6. The fluorescence intensity change of DPBF at 455 nm with the irradiation times (0 – 100 s) of 650 nm CW light beam (10 mW). (A) For the AuNR@SiO_2-Ce6 aqueous solution without pre-irradiation of 780 nm laser. (B) For the AuNR@SiO_2-Ce6 sample which has been pre-irradiated by 780 nm laser with the light dose of 2 J. (C) The DBPF degradations for AuNR@SiO_2-Ce6 samples which have been pre-irradiated by 780 nm laser with different doses. The excitation for DPBF fluorescence was 405 nm.

The controllable photosensitization ability of AuNR@SiO_2-Ce6 was subsequently studied in vitro. Cells were incubated with AuNR@SiO_2-Ce6 (20 pM-5 μM) for 3 h. Before the 650 nm light irradiation for PDT killing, these composite loaded cell samples in the wells of a 96 wells culture plate were pre-irradiated with different dose of 250 mW/cm^2 780 nm laser, respectively. Then after 650 nm light irradiation, cell samples were measured by the MTT assay. Figure 7A and 7B show the corresponding PDT results on KB and Hela cells. When the composite loaded cells were not pre-irradiated with 780 nm laser, the PDT damaging was neglectable. It could be understood as the bound Ce6 in AuNR@SiO_2-Ce6 is a poor $^1O_2$ generator as shown in Figure 6. For the cell samples which have been pre-irradiated with 780 nm laser, the PDT effect occurred and its killing efficiency was proportional to the irradiation dose of 780 nm pre-irradiation. The consistent PDT results on both KB and Hela cells confirmed that the 780 nm light could rule over the PDT effect of AuNR@SiO_2-Ce6 by controlling the Ce6 release. In addition, according to the purple columns, when cell samples were pre-irradiated by the 780 nm laser with the high dose of 5.6 J/cm^2 but not irradiated with the 650 light beam, the damaging effects on these cells were very slight compared with the control group. This result indicates that the 780 nm laser irradiation with the power density of 250 mW/cm^2 can photo-release the Ce6 from cellular AuNR@SiO_2-Ce6 but not directly damage the cells. The 780 nm is a NIR wavelength in the optical window region of living body. The NIR lights were found to be safe for living systems. Therefore using NIR light to control the drug release from metal nanoparticles could be a promising way of controlled drug release.

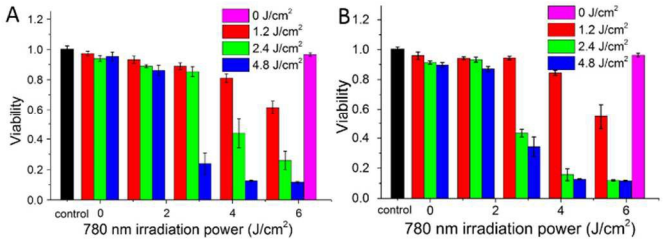

Fig. 7. The relationship of the cell viability without (the control group shown as the black bars) and with the pre-irradiation dose of 780 nm laser. Cells have been incubated with AuNR@SiO_2-Ce6 and irradiated by 650 nm light (10 mW/cm^2) to carry out PDT. (A) KB cells; (B) Hela cells. The incubation concentration of AuNR@SiO_2-Ce6 was 20 pM-5 μM. The values of 780 nm irradiation dose are 0, 1.4, 2.8, 4.2 and 5.6 J/cm^2 accordingly.

3. Experimental Section

3.1. Materials

The $HAuCl_4$, Hexadecyltrimethylammonium bromide (CTAB), $NaBH_4$, $AgNO_3$, L-ascorbic, (3-aminopropyl) triethoxysilane (APTES), Tetraethyl orthosilicate (TEOS) and ethyl acetate (EtoAc) were obtained from Sigma-Aldrich. Ce6 was obtained from Frontier Scientific, Logan, UT, USA. NaOH was obtained from Aladdin Industrial Inc. The D.I. water was self-produced with ions resin. 3-Diphenylisobenzofuran (DPBF) was obtained from J&K Chemical.

Hela cells (human epithelial cervical cancer cell line) and KB cells (a sub-line of the keratin-forming tumor cell line) were obtained from the cell bank of Shanghai Science Academy. Dulbecco's modified eagle medium (DMEM), Fetal bovine serum, 0.25% trypsin-EDTA (1x), Phosphate-Buffered Saline (PBS) and penicillin streptomycin were obtained from

Gibco. WST-1 (a Cell Proliferation and Cytotoxicity Assay Kit), was obtained from Beyotime.

3.2. Synthesis of AuNRs

According to the silver mediated method published[26-31], the AuNRs were synthesized. It can be separated into two steps. Firstly, synthesis of gold nanoseeds: $HAuCl_4$ (20 mM, 125 μL) and CTAB (0.1 M, 7.5 mL) were added into a 10-mL glass bottle with gentle mixing before the freshly prepared and ice-bathed $NaBH_4$ solution (10 mM, 0.6 mL) was injected, then the mixture was magnetically stirred until the color changed from golden yellow into brown which means the 3.5 nm gold nanoseeds were obtained. The seed solution was then kept at 27℃ for at least 2 hours before usage. Secondly, growth of gold nanorods: $HAuCl_4$ (20 mM, 250 μL) and $AgNO_3$ (10 mM, 100 μL) were added into CTAB (0.1 M, 10 mL) in a 20-mL glass bottle, followed by the addition of L-ascorbic acid (0.1 M, 60μL) and the 10 times diluted gold seeds (120 μL). The growth solution was left at 27℃ for overnight. Finally, the CTAB stabilized AuNRs were prepared.

3.3. Coating AuNRs with mesoporous silica shell

Silica-coated gold nanorods were produced from CTAB-stabilized gold nanorods by utilizing the surface CTAB on AuNRs as a silane coupling agent for mesoporous silica coating. Through a process of hydration and condensation of TEOS, a silica layer can be formed on the surface of AuNRs according to the established method[32-34]. The sample solution was centrifuged twice to wipe out superfluous CTAB and then re-dispersed in 30 mL of deionized (D.I.) water, because excess CTAB may prevent deposition of a uniform silica shell onto the AuNRs[35]. When the pH value of this solution was adjusted to about 10 with NaOH solution under stirring, 10 μL of tetraethyl orthosilicate (TEOS) together with 10 μL of APTES were subsequently injected slowly under vigorous stirring for 30 min and then this course was repeated twice. The reaction mixture was allowed to proceed for a few hours to form an approximately 11 nm thick silica layer on the surface of the AuNRs. Finally the AuNR@SiO_2 nanoparticles were isolated by centrifugation and washing with D.I. water several times, and then re-dissolved in D.I. water for further use. In the reaction course, the surface CTAB on the AuNRs works as moulds to form a mesoporous structure, enlarging the surface for more molecules to be adsorbed. The APTES provides amidogen on the silica shell, rendering the surface positively charged. Such a positively charged shell can improve the colloidal and shape stability of the nanorods.

3.4. Synthesis of mesoporous silica nanoparticles

Mesoporous silica nanoparticles (MSNs) were synthesized according to the method reported[36-42]. The 0.2 g CTAB was dissolved in 100 mL of D.I. water before 0.6 mL 2 M NaOH solution was added. The mixture was heated to 70 ℃ by oil heating bath under vigorous magnetic stirring for 10 min. Then 1 mL of TEOS together with 100 μL APTES was added to mix for a few minutes. 1 mL of EtoAc was continuously added and waited for another 30 s. The solution was left undisturbed for more than 2 h. Then the MSNs were obtained after centrifugation and washing with ethanol for 3 times. Since the amidogen was contained in mesoporous silica structure, these MSNs were also positively charged.

3.5. The preparation of composites

The molecular structure of Ce6 as is shown in Figure 1 E, shows the existence of carboxyl group. Each Ce6 molecule possesses 3 negative electron charges, under the condition of complete ionization. Therefore, the composites of Ce6 with above nanoparticles are easy to form due to the strong electrostatic attraction between the positive charged nanoparticles and the negative charged Ce6 molecules. The composites of AuNR-Ce6, AuNR@SiO_2-Ce6 and MSN-Ce6 were prepared by mixing 1 mL 20 pM AuNRs, AuNR@SiO_2 or MSNs with 5 μL 1mM Ce6 in dark and then shaken on a votex for overnight. Then the mixture was centrifuged to remove the un-conjugated Ce6 and re-suspend in aqueous solution for the subsequent usage.

3.6. Characterization of nanoparticles

By Agilent 8453 UV–visible/NIR spectrophotometer using quartz cuvettes of 10 mm optical path length, the absorption spectra of Ce6 and composites aqueous solutions were measured. The TEM images were taken by placing samples on carbon coated copper grids with a JEM-2100 transmission electron microscope operated at an accelerating voltage of 200 kV. Zeta potential was measured in the Malvern Zetasizer Nano S90 with a standard 633 nm laser.

3.7. Fluorescence measurements in solution

The fluorescence spectra were measured in a spectrometer (Hitachi, F-2500) with a 10 mm optical path quartz cuvette. The fluorescence lifetime time was measured with the method of Time-Correlated Single Photon Counting (TCSPC), which is based on the detection of single photons of a periodical light signal. A 2×10^7 Hz 405 nm Pico-second (ps) laser (Edinburgh Instruments, EPL405) was used for the excitation. The fluorescence decay courses were measured by a PMT (Hamamatsu, R928P) with a band-pass filter of 665±15 nm in the TCSPC (Edinburgh Instruments, TCC900). The obtained decay curves can be fitted with multi-exponential decay as described in formula (4), due to the fact that plasma intensity, which affects the radiation relaxation, is depended on the position with respect to the AuNRs [20, 43].

$$I(t) = \sum_{i=1}^{n} \alpha_i \exp\left(-\frac{t}{\tau_i}\right) \quad (4)$$

where $\boldsymbol{\tau_i}$ and $\boldsymbol{\alpha_i}$ represent the decay constant and amplitude of each exponential component, respectively. The average lifetime $\bar{\boldsymbol{\tau}}$ can be obtained according to formula (5) [25]

$$\bar{\boldsymbol{\tau}} = \frac{\sum_{i=1}^{n} \alpha_i \tau_i^2}{\sum_{i=1}^{n} \alpha_i \tau_i} \quad (5)$$

With the numerous measurements, the average fluorescence lifetimes of Ce6 in different cases were determined.

3.8. Cell culture

Cells were maintained in DMEM medium with 10% calf serum, 100 units/mL penicillin, 100 μg/mL streptomycin and 100 μg/mL neomycin in a humidified standard incubator with a 5% CO_2 atmosphere at 37 ºC. When the cells reached 80% confluence with normal morphology, the tested compound was added in and the cells were incubated in the incubator for 3 hours for the case of conjugates of AuNR@SiO_2-Ce6 or MSNs-Ce6 and 5 hours for free Ce6. After that, these cells were washed three times with PBS. Then the cell samples were ready for fluorescence imaging measurements and fluorescence lifetime imaging measurements.

3.9. Fluorescence intensity imaging and fluorescence lifetime imaging

The fluorescence imaging of Ce6 in cells was acquired in a laser scanning confocal microscope (Olympus FV300, IX 71) equipped with a matched pinhole and a band-pass filter of 660±15 nm in the detection channel. A water immersion objective (UplanApo, 60X, and 1.2 NA) was used in these measurements. A 405 nm continuous wave (CW) laser was used for common imaging excitation. Differential interference contrast (DIC) images were recorded simultaneously in a transmission channel to exhibit the cell morphology.

The FLIM images of these composite loaded cells were acquired in parallel. The FLIM (Becker & Hickl GmbH. BDL-405-SMC ps laser, PMC-100 detector under the control of SPC-150 board and DCC-100) system was installed on the top cap of Olympus FV300 by replace the dichroscope with a reflector. Under XY repeat model, those fluorescence photons from Ce6 excited by a 405 nm ps laser at a repetition rate of 20 MHz got passed through a 660±15 nm band-pass filter in the confocal fluorescence microscopy system to be collected by a photon counter (PMC-100). Then the lifetime of each pixel was figured out by fitting the intensity decay with the following exponential decay function.

$$I(t) = \mathrm{I}_0 + A_1 \exp\left(-\frac{t}{\tau_1}\right) + A_2 \exp\left(-\frac{t}{\tau_2}\right) \quad (6)$$

Then according to formula (5) the intensity-weighted average lifetime (τ) of every pixel was calculated standing for the lifetime of corresponding pixel. After XY repeat scanning of the 405 nm ps laser, the FLIM image was established.

3.10. Cytotoxicity of Ce6, and Ce6 composites

WST-1 was used to measure the dark toxicity of Ce6, AuNRs, MSNs and Ce6 composites on cells. 200 μL cell suspension with a consistency of 10^3 cells per mL was seeded in each well of a 96-well flat bottom tissue culture plat and allowed to attach to the plat and proliferate. When the cells reached 80% confluence with normal morphology, the Ce6 (5 μM), AuNR-Ce6 (20 pM -5 μM), AuNR@SiO_2-Ce6 (20 pM-5μM) or MSN-Ce6 (20 pM-5 μM) composites were added into corresponding wells, respectively, and incubated for the desired time. Then, the cells were incubated in 100 μL DMEM with 10 μL MTT solution (5 mg/mL) for another 2 h. Finally, the optical densities (O.D) at 450 nm of each well were measured in an iEMS Analyzer (Lab-system). The cell viability in each well was determined by comparing the O.D value with that of untreated control cells in other wells of the same plate. All results were presented as the mean ± SE from three independent experiments with 6 wells in each.

3.11. Singlet oxygen ($^1O_2$) measurements

DPBF, a sensitive $^1O_2$ probe, was used to measure the $^1O_2$ photo-produced by Ce6 in different situations. Upon oxidative degradation by $^1O_2$, the fluorescence of DBPF was quenched, so that the reducing rate of DPBF fluorescence in the sample solution is proportional to the $^1O_2$ production. In the experiment the DBPF (10 mM) was added into the sample solution. The 10 mW 660±15 nm light was used to irradiate the sample solutions at a 20s interval. Then the fluorescence of DBPF was measured accordingly to quantify the relative $^1O_2$ production.

3.12. PDT effect of released Ce6 from AuNR@SiO_2-Ce6 on cells

A culture plate with 96 wells, previously seeded in each well with 200 μL cells with concentration of 3×10^3 cells/ mL, was used in this experiment. When the cells reached 80% confluence with normal morphology, the AuNR@SiO_2-Ce6 (20 pM-5 μM) was added into each well and incubated for 3 h. After incubation, the cells were washed with PBS three times and replenished with fresh medium. Then these cell wells were irradiated by a 780 nm laser (OEWindw MOGlabs) with power density of 250 mW/cm^2 for desired times for different wells to make the Ce6 released from cellular AuNR@SiO_2-Ce6 composites. After that, the cell wells were further irradiated by a CW light beam (660±15 nm) with the power density of 10 mW/cm^2 to carry out the Ce6 mediated PDT. After the irradiation, the cells were incubated for another 24 h. Then, the cells were incubated in 100 μL DMEM with 10 μL MTT solution (5 mg/mL) for 2 h. Finally, the O.D at 450 nm of each well were measured in an iEMS Analyzer (Lab-system). The cell viability in each well was determined by comparing the O.D value with that of untreated control cells in some wells of the same plate. All results were presented as the mean ± SE from three independent experiments with 6 wells in each.

Conclusions

The mesoporous silica shell of AuNR@SiO_2 contained amidogen so that the Ce6 molecules were easy to be conjugated on AuNRs to form AuNR@SiO_2-Ce6 with the loading efficiency of 80%. Due to the strong absorption of AuNRs at LSPR band, the 780 nm laser can heat the AuNR@SiO_2-Ce6 to release Ce6 making AuNR@SiO_2-Ce6 a photo-controllable Ce6 releasing composite. The fluorescence lifetime of conjugated Ce6 in AuNR@SiO_2-Ce6 was remarkably shortened to 0.9 ns in contrast to that of 6 ns when released. Utilizing the fluorescence lifetime difference between the conjugated Ce6 and free Ce6, we developed FLIM technique to measure the photo-controllable Ce6 release from AuNR@SiO_2-Ce6 in living cells with a 780 nm laser. We found that the 780 nm laser beam can not only control the releasing amount of Ce6 from cellular AuNR@SiO_2-Ce6 by adjusting the irradiation dose of 780 nm laser but also precisely control the micro-region of Ce6 release in the cell by focusing the laser beam on the selected site. The free Ce6 is an efficient photosensitizer, whereas the PDT activity of AuNR@SiO_2-Ce6 is low because the $^1O_2$ generation ability of AuNR@SiO_2-Ce6 is remarkably limited. Therefore, controlling the Ce6 release of AuNR@SiO_2-Ce6 with 780 nm laser can control the PDT effect of AuNR@SiO_2-Ce6, which is confirmed in PDT killing experiments on both KB and Hela cells. We believe the controllable PDT effect has great potentials in PDT practices by releasing photosensitizers on tumour sites only and thus preventing the skin photo-toxicity.

Acknowledgments

Financial support from the National Natural Science Foundation of China (11074053 and 31170802) is gratefully acknowledged.

Notes and references

State Key Laboratory of Surface Physics and Department of Physics, and Key Laboratory of Micro and Nano Photonic Structures (Ministry of Education), Fudan University, Shanghai 200433, China.

Address: No. 220 on Handan road in Yanpu district of Shanghai, 200433,China
*email: because of the tragic sudden pass-away of professor J. Chen, correspondences should be sent to Y. Xu at 12110190045@fudan.edu.cn, or M. Ji at minbiaoj@fudan.edu.cn

1. D. Pissuwan, T. Niidome and M. B. Cortie, *Journal of Controlled Release*, 2011, 149, 65-71.
2. J. L. Vivero-Escoto, Slowing, II, C. W. Wu and V. S. Y. Lin, *Journal of the American Chemical Society*, 2009, 131, 3462-3463.
3. Y. N. Zhao, B. G. Trewyn, Slowing, II and V. S. Y. Lin, *Journal of the American Chemical Society*, 2009, 131, 8398-8400.
4. K. K. Coti, M. E. Belowich, M. Liong, M. W. Ambrogio, Y. A. Lau, H. A. Khatib, J. I. Zink, N. M. Khashab and J. F. Stoddart, *Nanoscale*, 2009, 1, 16-39.
5. Z. J. Zhang, L. M. Wang, J. Wang, X. M. Jiang, X. H. Li, Z. J. Hu, Y. H. Ji, X. C. Wu and C. Y. Chen, *Advanced Materials*, 2012, 24, 1418-1423.
6. T. Luo, P. Huang, G. Gao, G. X. Shen, S. Fu, D. X. Cui, C. Q. Zhou and Q. S. Ren, *Optics Express*, 2011, 19, 17030-17039.
7. C. D. S. Brites, P. P. Lima, N. J. O. Silva, A. Millan, V. S. Amaral, F. Palacio and L. D. Carlos, *Nanoscale*, 2012, 4, 4799-4829.
8. J. A. Webb and R. Bardhan, *Nanoscale*, 2014, 6, 2502-2530.
9. C. Y. Li and J. F. Zhu, *Materials Letters*, 2013, 112, 169-172.
10. J. Malicka, I. Gryczynski and J. R. Lakowicz, *Biochemical and Biophysical Research Communications*, 2003, 306, 213-218.
11. J. Chen, Y. H. Jin, N. Fahruddin and J. X. Zhao, *Langmuir*, 2013, 29, 1584-1591.
12. X. Li, F. J. Kao, C. C. Chuang and S. L. He, *Opt. Express*, 2010, 18, 11335-11346.
13. X. H. Huang, P. K. Jain, I. H. El-Sayed and M. A. El-Sayed, *Lasers in Medical Science*, 2008, 23, 217-228.
14. E. B. Dickerson, E. C. Dreaden, X. H. Huang, I. H. El-Sayed, H. H. Chu, S. Pushpanketh, J. F. McDonald and M. A. El-Sayed, *Cancer Letters*, 2008, 269, 57-66.
15. S. H. Yong-Kui Xu , Sungjee Kim and Ji-Yao Chen, *ACS Applied Materials & Interfaces*, 6, 10.
16. X. Wu, J. Y. Chen, A. Brech, C. H. Fang, J. F. Wang, P. J. Helm and Q. Peng, *Biomaterials*, 2013, 34, 6157-6162.
17. G. M. Santos, F. S. Zhao, J. B. Zeng and W. C. Shih, *Nanoscale*, 2014, 6, 5718-5724.
18. Z. Zhang, J. Wang, X. Nie, T. Wen, Y. Ji, X. Wu, Y. Zhao and C. Chen, *Journal of the American Chemical Society*, 2014, 136, 7317-7326.
19. W. Li, X. Cai, C. Kim, G. Sun, Y. Zhang, R. Deng, M. Yang, J. Chen, S. Achilefu, L. V. Wang and Y. Xia, *Nanoscale*, 2011, 3, 1724-1730.
20. N. S. Abadeer, M. R. Brennan, W. L. Wilson and C. J. Murphy, *ACS Nano*, 2014, 8, 8392-8406.
21. B. Stella, S. Arpicco, M. T. Peracchia, D. Desmaele, J. Hoebeke, M. Renoir, J. D'Angelo, L. Cattel and P. Couvreur, *Journal of Pharmaceutical Sciences*, 2000, 89, 1452-1464.
22. W. C. Chen, A. X. Zhang and S.-D. Li, *European Journal of Nanomedicine*, 2012, 4, 89-93.
23. K. Greish, *Journal of Drug Targeting*, 2007, 15, 457-464.
24. A. Samanta, Y. D. Zhou, S. L. Zou, H. Yan and Y. Liu, *Nano Letters*, 2014, 14, 5052-5057.
25. R. Yasuda, C. D. Harvey, H. N. Zhong, A. Sobczyk, L. van Aelst and K. Svoboda, *Nature Neuroscience*, 2006, 9, 283-291.
26. S. Eustis and M. El-Sayed, *Journal of Physical Chemistry B*, 2005, 109, 16350-16356.
27. M. A. Mahmoud and M. A. El-Sayed, *Journal of Physical Chemistry Letters*, 2013, 4, 1541-1545.
28. M. B. Mohamed, V. Volkov, S. Link and M. A. El-Sayed, *Chemical Physics Letters*, 2000, 317, 517-523.
29. W. Ni, X. Kou, Z. Yang and J. Wang, *ACS Nano*, 2008, 2, 677-686.
30. T. K. Sau and C. J. Murphy, *Journal of the American Chemical Society*, 2004, 126, 8648-8649.
31. J. E. Park, M. Atobe and T. Fuchigami, *Ultrasonics Sonochemistry*, 2006, 13, 237-241.
32. Y. S. Chen, W. Frey, S. Kim, P. Kruizinga, K. Homan and S. Emelianov, *Nano Letters*, 2011, 11, 348-354.
33. J. V. Jokerst, M. Thangaraj, P. J. Kempen, R. Sinclair and S. S. Gambhir, *ACS Nano*, 2012, 6, 5920-5930.
34. X. J. Tian, J. Guo, Y. Tian, H. Y. Tang and W. L. Yang, *RSC Advances*, 2014, 4, 9343-9348.
35. Y. Lu, Y. D. Yin, Z. Y. Li and Y. N. Xia, *Nano Letters*, 2002, 2, 785-788.
36. J. Kim, H. S. Kim, N. Lee, T. Kim, H. Kim, T. Yu, I. C. Song, W. K. Moon and T. Hyeon, *Angewandte Chemie-International Edition*, 2008, 47, 8438-8441.
37. J. Lu, M. Liong, J. I. Zink and F. Tamanoi, *Small*, 2007, 3, 1341-1346.
38. Slowing, II, B. G. Trewyn, S. Giri and V. S. Y. Lin, *Advanced Functional Materials*, 2007, 17, 1225-1236.
39. Slowing, II, B. G. Trewyn and V. S. Y. Lin, *Journal of the American Chemical Society*, 2007, 129, 8845-8849.
40. Slowing, II, J. L. Vivero-Escoto, C. W. Wu and V. S. Y. Lin, *Advanced Drug Delivery Reviews*, 2008, 60, 1278-1288.
41. F. Torney, B. G. Trewyn, V. S. Y. Lin and K. Wang, *Nature Nanotechnology*, 2007, 2, 295-300.
42. J. L. Vivero-Escoto, Slowing, II, B. G. Trewyn and V. S. Y. Lin, *Small*, 2010, 6, 1952-1967.
43. S. Khatua, P. M. R. Paulo, H. F. Yuan, A. Gupta, P. Zijlstra and M. Orrit, *ACS Nano*, 2014, 8, 4440-4449.